ChemSusChem

Research Article
doi.org/10.1002/cssc.202300971

Chemistry Europe
European Chemical Societies Publishing

www.chemsuschem.org

Zwitterionic "Solutions" for Reversible CO_2 Capture

Guilherme L. P. Aydos,*[a] Graciane Marin,[a] Günter Ebeling,[a] Francisco P. dos Santos,[a] Bárbara C. Leal,[a] Rafael D. Zink,[a] Brenda A. Vargas,[a] Pedro Migowski,[a] Rafael Stieler,[a] Bruno B. de Araújo,[a] Paulo Gonçalves,[a] Hubert K. Stassen,[a] Leonardo dos Santos Pereira,[b] Ana Paula Musse,[b] and Jairton Dupont*[a]

The zwitterions resulting from the covalent attachment of 3- or 4-hydroxy benzene to the 1,3-dimethylimidazolium cation represent basic compounds (pKa of 8.68 and 8.99 in aqueous solutions, respectively) that chemisorb in aqueous solutions 0.58 mol/mol of carbon dioxide at 1.3 bar (absolute) and 40 °C. Equimolar amounts of chemisorbed CO_2 in these solutions are obtained at 10 bar and 40 °C. Chemisorption takes place through the formation of bicarbonate in the aqueous solution using imidazolium-containing phenolate. CO_2 is liberated by simple pressure relief and heating, regenerating the base. The enthalpy of absorption was estimated to be −38 kJ/mol, which is about 30% lower than the enthalpy of industrially employed aqueous solutions of MDEA (estimated at −53 kJ/mol using the same experimental apparatus). The physisorption of CO_2 becomes relevant at higher pressures (>10 bar) in these aqueous solutions. Combined physio- and chemisorption of up to 1.3 mol/mol at 40 bar and 40 °C can be attained with these aqueous zwitterionic solutions that are thermally stable and can be recycled at least 20 times.

Introduction

The choice of a specific CO_2 capture technology heavily depends on the type of the process that generates the CO_2.[1] Among the available CO_2 separation processes, sorption is most commonly adopted due to its higher efficiency and lower cost.[2] This process is especially important in post-combustion industrial processes to remove CO_2 from gas streams. In this case, the chief technology currently used is based on reversible sorption using aqueous solutions of alkanolamines, such as N-methyl-diethanolamine (MDEA) associated with piperazine.[3] Although they are effective, there are serious drawbacks intrinsically related to their physico-chemical properties, such as thermal and chemical stability (volatilization, oxidative degradation of the amine leading to environmental issues), the high energy required to operate the separation process, corrosion of tubes and the consequent increase in production costs.[4] Among the various approaches to the search for new alternatives for reversible CO_2 capture, ionic liquids (ILs) have been widely investigated recently.[1a,5] There is an increasing number of publications reporting the use of these salts in CO_2 sorption processes and more than 100 ILs have been projected as promising solvents for CO_2 capture.[1a,6] The most remarkable property which makes these fluids attractive for numerous processes is their negligible vapor pressure.[7] Thus, ILs potentially mitigate the environmental concerns associated with the use of traditional volatile solvents such as ethanolamines.[8] However, the use of traditional ILs as physical sorbents for CO_2 is limited by the high molecular weight of these compounds presenting high viscosity and density.[9] ILs containing basic moieties either at the cation or anion are capable to chemisorb CO_2. For example, ILs with imidazolium cations containing an amino group are able to capture 0.5 moles of CO_2 per mole of IL under ambient pressure.[10] Indeed, many publications describe the use of ILs with such as amino-, azolate-, alcoholate- and phenolate-moieties.[11] When water is present, the functional groups form mainly bicarbonates but also may form O–CO_2 or N–CO_2 adducts depending on the functional group present.

Although a significant amount of progress has been achieved, several drawbacks should be mentioned: high viscosity of the ILs, complex synthesis and potentially higher energy demands in the desorption step due to the formation of carbamate like adducts. Thus, from a practical point of view, these sorbents cannot be easily substituting the aqueous amine solutions in industrial plants.

To solve such problems, the development of an ideal liquid sorbent (Figure 1) continues an emergent trend. The challenge is to develop small molar mass and non-volatile sorbents dissolved in water with low viscosity and similar molar sorption capacity of conventional sorbents. It is also important that the sorbent solution is less corrosive, and less susceptible to chemical and thermal decomposition as compared to alkanolamine solutions, as well as presenting a low sorption enthalpy. The present work is the result of our efforts in the development

[a] Dr. G. L. P. Aydos, Dr. G. Marin, Prof. G. Ebeling, Prof. F. P. dos Santos, Prof. B. C. Leal, R. D. Zink, B. A. Vargas, Prof. P. Migowski, Prof. R. Stieler, B. B. de Araújo, Prof. P. Gonçalves, Prof. H. K. Stassen, Prof. J. Dupont
Institute of Chemistry
Universidade Federal do Rio Grande do Sul–UFRGS
Av. Bento Gonçalves, 9500 Porto Alegre 91501-970 RS (Brazil)
E-mail: guilherme.aydos@ufrgs.br
jairton.dupont@ufrgs.br

[b] L. dos Santos Pereira, Dr. A. P. Musse
Petrobras/CENPES
Cidade Universitária, Ilha do Fundão, Avenida Horácio Macedo 950, Rio de Janeiro, RJ, CEP, 21941–915 (Brazil)

Supporting information for this article is available on the WWW under https://doi.org/10.1002/cssc.202300971

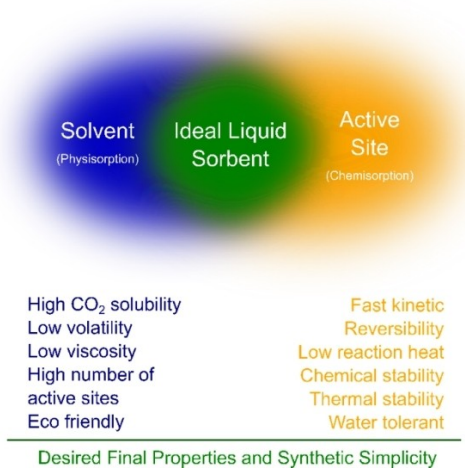

Figure 1. Properties of an ideal liquid CO_2 sorbent.

of sorbents that may overcome the intrinsic problems of alkanolamine solutions in the capture processes of CO_2 from gas streams.[12] Herein we present the design, synthesis, and use of new zwitterionic compounds that are non-volatile, thereby eliminating the loss of sorbent mass in the desorption stage of traditional industrial CO_2 capture processes. This new class of basic zwitterionic compounds provides opportunities for future studies in the search of more efficient systems by partially or completely replacing current amine-based aqueous solutions in CO_2 capture processes.

Results and Discussion

Considering that aqueous solutions of alkanolamines are the most widely used fluids for CO_2 absorption processes, the starting point was to focus on designing compounds that fulfil the active site criteria illustrated in Figure 1. These criteria include fast kinetics, reversibility, low heat of reaction, chemical stability, thermal stability, and water tolerance. In principle, such compounds could allow for the upgrade of existing industrial plants by simply replacing the alkanolamines currently in use.

It is well known that the order of absorption heat for different types of amines is primary > secondary > tertiary functional groups in aqueous solutions.[13] The CO_2 capture by aqueous solutions of sterically hindered amines does not form carbamates and its mechanism can be well explained by base-catalyzed CO_2 hydration.[14] Regardless of the reaction mechanism, the strength of the base is strongly related to the kinetics and energy of the reaction.[15] Hence, our first intention was to design a non-volatile compound that would act as a base in an analogous way to tertiary amines, particularly MDEA. For this reason, we investigated the acid-base equilibrium of CO_2 absorption in an aqueous solution of a hypothetical base to estimate a pKa (conjugated acid) range of interest at this stage.

The equilibrium involved in the capture and release of CO_2 by aqueous solutions of basic compounds can be thought of as in equations (1) to (6):

$$B_{(aq)} + H_2CO_{3(aq)} \rightleftharpoons BH^+_{(aq)} + HCO^-_{3(aq)} \quad (1)$$

$$K_1 = \frac{\left[BH^+_{(aq)}\right].[HCO^-_{3(aq)}]}{[H_2CO_{3(aq)}].[B_{(aq)}]} \quad (2)$$

$$BH^+_{(aq)} + H_2O_{(l)} \rightleftharpoons B_{(aq)} + H_3O^+_{(aq)} \quad (3)$$

$$K_{conj} = \frac{\left[B_{(aq)}\right].[H_3O^+_{(aq)}]}{\left[BH^+_{(aq)}\right]} \quad (4)$$

$$H_2CO_{3(aq)} + H_2O_{(l)} \rightleftharpoons HCO^-_{3(aq)} + H_3O^+_{(aq)} \quad (5)$$

$$K_{a1} = \frac{[HCO^-_{3(aq)}].[H_3O^+_{(aq)}]}{[H_2CO_{3(aq)}]} \quad (6)$$

The equilibrium constant of reaction (1), K_1, is given by the ratio of the first ionization constant of carbonic acid (K_{a1}) and the ionization constant of the conjugated acid (K_{conj}) of the base B. Therefore, the concentration of products in equilibrium (1) will be higher as weaker acids are formed from the protonation of the base by H_2CO_3. An almost complete reaction would be expected with K_{a1}/K_{conj} around 10^6. In other words, a difference in pKa of 6 units would give a virtually quantitative CO_2 capture by the base. One would think that choosing a stronger base is the best option for carbon capture. However, for the desorption step, it is necessary that some carbonic acid is present in equilibrium so that it can be decomposed back into $CO_{2(g)}$. This enable the CO_2 to leave the aqueous phase, shifting the equilibrium to regenerate the capturing base without incurring a high energy penalty Thus, the key point is to fine-tune the acidity of the conjugated acid of the capturing base that maximize the formation of bicarbonate and that can be deprotonated back to reform the base by HCO_3^-. A graph of the concentration of bicarbonate vs conjugated acid pKa was plotted and is shown in Figure 2. The curve was obtained considering an ideal solution with $CO_{2(g)}$ partial pressure of 1 bar, at room temperature (25 °C) and 1.00 mol/L base initial concentration and hence it was used only as a reference to choose the ideal pKa range.

The resolution of Equations (1) to (6) was performed using Maple 15 and bases with conjugated acids exhibiting pKa values between 8 and 10 were found to be ideal for the reversible sorption process (for details see Supporting Information). As shown in Figure 2, weaker bases lead to lower sorption, whereas stronger bases are expected to impair the desorption process.

Hence, the phenolate group was chosen as the active site, because it is one of the few alternatives to the amino group with basicity in the region of interest. The phenolate anion had already been reported as a promising alternative for amine-free CO_2 capture processes or blends.[17] One choice would be the

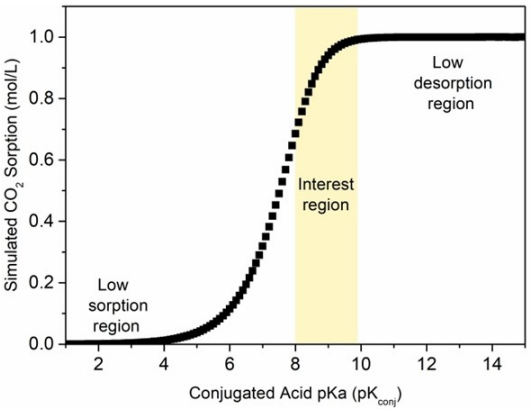

Figure 2. Simulation as a tool for the design of a basic CO_2 sorbent (B = base) using $K_{a1} = 3.2\times10^{-4}$ (the apparent equilibrium constant of H_2CO_3 is $pKa_1 = 6.5$ since the acid concentration depends on the $CO_{2(aq)}$ hydration constant).[16]

phenolate anion in a simple salt with sodium. However, it is not the best option as volatile and toxic phenol would be formed in the aqueous CO_2 capture. Alternatively, one can covalently attach an organic cation to the aromatic ring of a phenol,[18] so an internal salt is formed in the phenolate form and decrease base volatility. 1,3-dimethylimidazolium cations were easily attached to phenols to prepare zwitterions **3** and **4**, Scheme 1. Only three steps using classical methods such as condensation-cyclization, alkylation, and deprotonation were used. These compounds are the simplest of this family of zwitterionic salts, having the shortest imidazolium side chain to achieve the lowest molar mass and hypothetically the highest solubility in water. The overall yield was 37–51% (not optimized) on a scale of up to 0.5 kg.

Calculated pKa of 9.00 and 8.50 for **1** and **2**, respectively, were obtained from quantum-mechanical methods with a HF// 6-31G* level. This is in good agreement with those determined experimentally for the conjugate acids of **3** and **4** (8.99 and 8.68, respectively; see Figure S1 in Supporting Information). The zwitterions **3** and **4** were characterized by ^1H, ^{13}C NMR and UV-Vis spectroscopy, and single crystal X-ray diffraction analysis (see Supporting Information for further details).

NMR ^1H-^1H-NOESY studies (Figure S2) were performed to evaluate the molecular structure of both zwitterionic species **3** and **4** in aqueous solutions. The results evidence interaction with HDO through a higher relative cross-peak interaction between H_7 and H_{11} of the phenolate moiety in **3** or H_8 (phenolate) and H_4, H_5 and H_9 (imidazolium) in **4**. Only intra-zwitterionic interactions of H_{10} of the N-methyl groups with the H_4 and H_5 of the imidazolium ring as well as with the H_6 and H_7 of the phenolate are observed on NOESY of **3** (Figure 3a). Interestingly, inter-zwitterionic interactions were observed on the NOESY spectra of **4** (Figure 3b) through an interaction pattern with a higher cross-peak intensity, corresponding to higher relative cross-relaxation rates between H_7 and H_8 of the phenolate moiety and H_4 and H_5 of the imidazolium cation moiety. The interactions observed by NOESY experiments in organic solutions suggest a structural arrangement that is consistent with both X-ray diffraction analysis and DFT calculations (see below).

The X-ray structures of **3** and **4** clearly show that the phenolate group is not conjugated with the imidazolium ring, as evidenced by their orthogonal-like positions (refer to Figure 4). The torsion angle between the phenolate and imidazolium rings is 67.4° (**3**) and 46.2° (**4**) (average of two crystallographic independent molecules). These different orientations are probably due to steric constraints imposed by methyl groups of imidazolium ring and the positions (meta and para) of the O- moiety on the phenol ring for the packing. The C-imidazolium–C-phenolate distances of 1.476 and 1.452 Å (average of two crystallographic independent molecules) for **3** and **4**, respectively, fall within the range for carbon–carbon sp^2–sp^2 sigma bonds, which are usually around 1.47 Å.[19] The inter-zwitterionic distance between the centroids of the imidazolium and phenolate rings in **4** is 4.2689 Å, suggesting offset-stacked geometry ('electrostatic alignment'), which is typically observed with most aromatics.[20] The observed interaction between H_7 of the phenolate and H_4 of the imidazolium ring in the NOESY spectrum of **4** is also reflected in a short distance between these atoms (3.4727 Å), suggesting the inter-zwitterionic interactions in the crystalline solid (Figure S3b). In the case of **3** (Figure S3a), the H-interactions occur between the H of the imidazolium and the phenolate of the same zwitterion, being more pronounced between H_{10} (methyl groups) and H_7 (ortho) of the phenolate (2.6292 Å).

It was also observed in both structures (**3** and **4**) strong H-bonds between the zwitterions and the surrounding water molecules (O···H(D)$_2$O), with distances from 1.817 to 2.459 Å and D–H···A (D = donor, A = acceptor) angles from 143.72° to 178.84° for **3** and distances from 1.914 to 2.573 Å and angles between 142.42° and 178.03° for the zwitterion **4** (Figures S4 and S5).

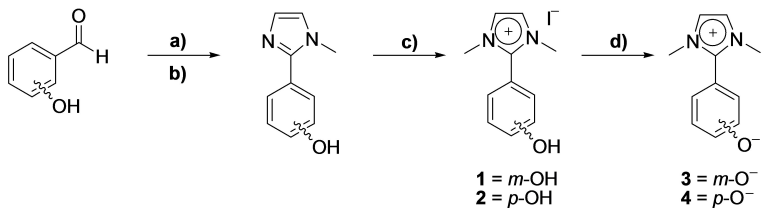

Scheme 1. a) $MeNH_2$ (40% aq), CH_3OH, R.T., 10 min. b) Glyoxal (40% aq), CH_3OH, $(NH_4)_2CO_3$, 0 °C–room temperature. c) CH_3I, CH_3CN, 70 °C, 1 h. d) AmberSep 900 OH, room temperature, 10 min.

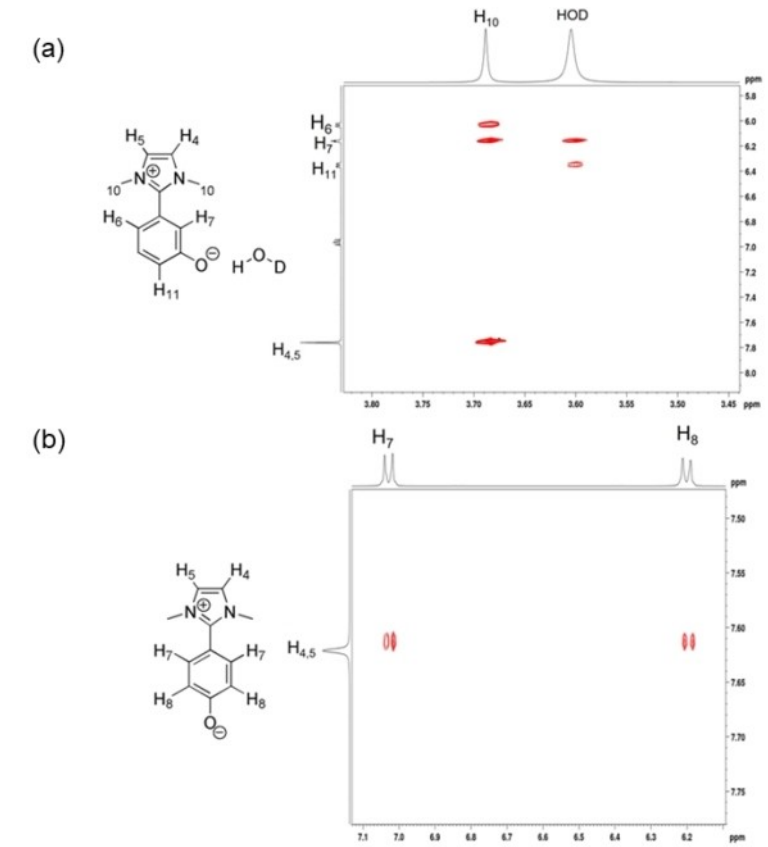

Figure 3. Expansion of the map contour of the NOESY spectrum (400 MHz) of **3** (a) and **4** (b) in DMSO-d_6 at 25 °C.

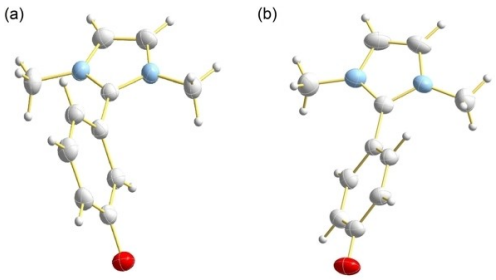

Figure 4. X-ray structure of **3** (a) and **4** (b). Blue = N, red = O, grey = C and H.

The DFT-derivative structures of **3** and **4** (Figure 5a and 5b, respectively) are consistent with experimentally results. In the calculated system formed by molecules of **4**, there is less deviation from the planarity compared to the system formed by molecules of **3**, since the angle between they imidazolium and phenolate rings are approximately 40° and 70°, respectively. This indicates a better interaction between the molecular pairs of **4**, as evidenced by the shorter distance between the imidazolium and phenolate rings (4.336 and 3.676 Å) compared to the system of **3** (6.309 and 4.185 Å). The nearest atoms in system of **4**, are the hydrogens of the aromatic ring and the hydrogen of the imidazolium methyl group of the neighbouring

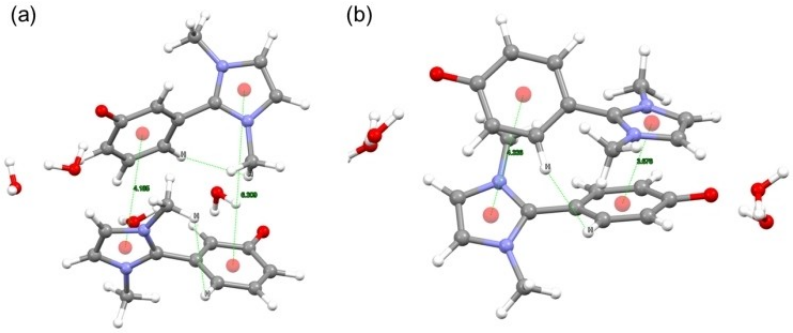

Figure 5. DFT calculations of **3** (a) and **4** (b). The shortest interactions are indicated by dashed lines: inter-zwitterionic in **4** and intra-zwitterionic in **3**. Blue = N, red = O, grey = C and light grey = H.

molecule, with 2.490 Å. In Figure 5a, the shortest distances between hydrogens occur in the same molecule of **3**, between the hydrogens of the methyl group of the imidazolium ring and the hydrogen of the (ortho)-phenolate, at 2.594 Å. The DFT calculations also confirm the interactions between H_2O and the phenolate moiety, corroborating NOESY and X-ray results. The obtained structural parameters confirm that the unit of **4** can be considered a dimer due to the effective interaction between the subunits. These computations also revealed that the intimate contact ion pair is adopted as a more stable configuration. Hence, in **4** the more stable unit can be described as a dimer i.e. $[\mathbf{4}]_2$ in the solid, gas and in even in solution. This behavior is another indication that the imidazolium compounds tend to organize as contact ion pairs or clusters, rather than as solvent-separated ions.[21] Although intermolecular interactions are less evident in **3**, cluster observed by electron spray ionization mass spectroscopy show that the dimeric form of **3** is the most abundant under analysis conditions, as shown in Figure S6c.

Solutions of **3** and **4** in water can be attained with concentrations up to 3.5–3.8 mol/L, which corresponds to the same range of concentrations used in industrial plants applying aqueous MDEA/piperazine technology.[2a] The TGA analysis of the commercial mixture MDEA/piperazine (Figure S7a) exhibits a gradual loss of mass from around 50 °C (due to the evaporation of the mixture components), until a temperature of approximately 200 °C (complete mass loss). On the contrary, **3** (Figure S7b) exhibits only a minor loss of mass (2.6%) from around 75 °C, due to the residual water, and begins to decompose only at 219 °C.

The CO_2 sorption/desorption cycle in aqueous solutions of **3** and **4** was investigated by ^{13}C NMR. The spectra show only the formation of bicarbonate (159.1 ppm[7]) at lower pressures (1.3 bar) and no signal indicating the decomposition of imidazolium species, corroborating the reversibility of the system after thermal desorption, regenerating the zwitterion and liberating the CO_2 gas (see Figure 6). Note that in the desorption process employed at 100 °C, some of the bicarbonate is still present after the desorption by pressure release. The sorption/desorption cycle was also corroborated by UV-Vis spectroscopy. The absorption maximum of **3** is located around 306 nm and is related to a charge transfer process. After CO_2 sorption, this band disappears and a new band arises at 283 nm, which is ascribed as phenol form **1**. The charge transfer band is restored after desorption step, due to the regeneration of **3**. The phenols decreases the energy needed for the π-π* electronic transition due to the conjugation of the negative charge of oxygen atom with the aromatic ring.[22] In addition, the maxima of absorption of phenolate **3** blue shifts from 231 to 220 nm and showed a bathochromic effect back to 231 nm after desorption at 100 °C (Figure S8).

Using quantitative high-pressure NMR HP-^{13}C NMR (from 10 to 40 bar) a sorption of 1.3 mol of CO_2/mol of **3** was attained at 40 bar and 40 °C (Figure S9). CO_2 physisorption is only detectable at pressures $\geq$ 10 bar and shows peaks between 121.9 and 123.3 ppm. Besides solvated CO_2, the only species detected were bicarbonate and the phenol **1** or **2**. The possible presence of phenylcarbonates in the aqueous solution was investigated through HMBC studies (Figure S10) and did not find these species under any circumstances. This is in contrast with previous reports[11j,23] that showed the formation of phenylcarbonates in ILs with 0.1% of water. Therefore, in aqueous solutions, phenolate anion probably reacts with water and CO_2 to form bicarbonate and the direct nucleophilic attack of phenolate to CO_2 is unlikely.

Two different pathways of CO_2 chemisorption in aqueous solutions of **3** were considered (Scheme 2).

Path I involves the direct protonation of **3** by carbonic acid, resulting in the production of **1** with bicarbonate ion. It was

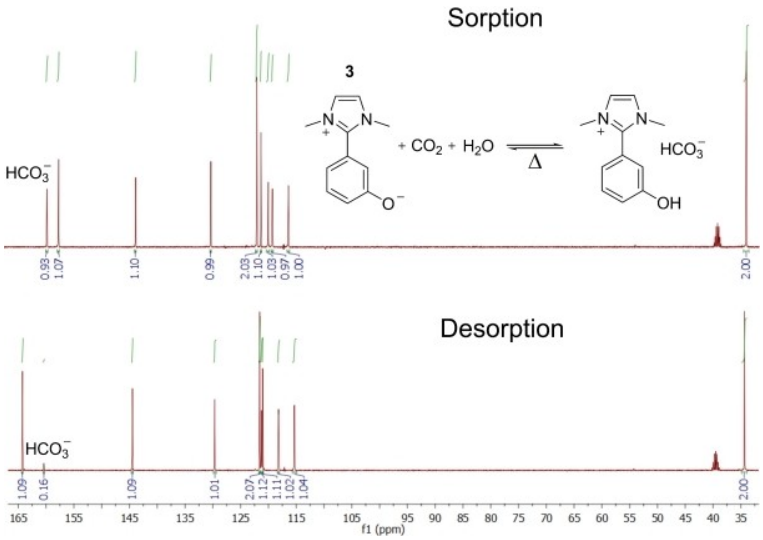

Figure 6. ^{13}C NMR spectra (using a DMSO-d_6 capillary as internal standard) of the adsorption (40 °C, 1.3 bar)/desorption (100 °C, atmospheric pressure) of CO_2 by a 1.0 M aqueous solution of **3** (first run). The peak at 159.1 ppm corresponds to bicarbonate and no sign of physiosorbed CO_2 that usually appears at 122–124 ppm was observed at this pressure.

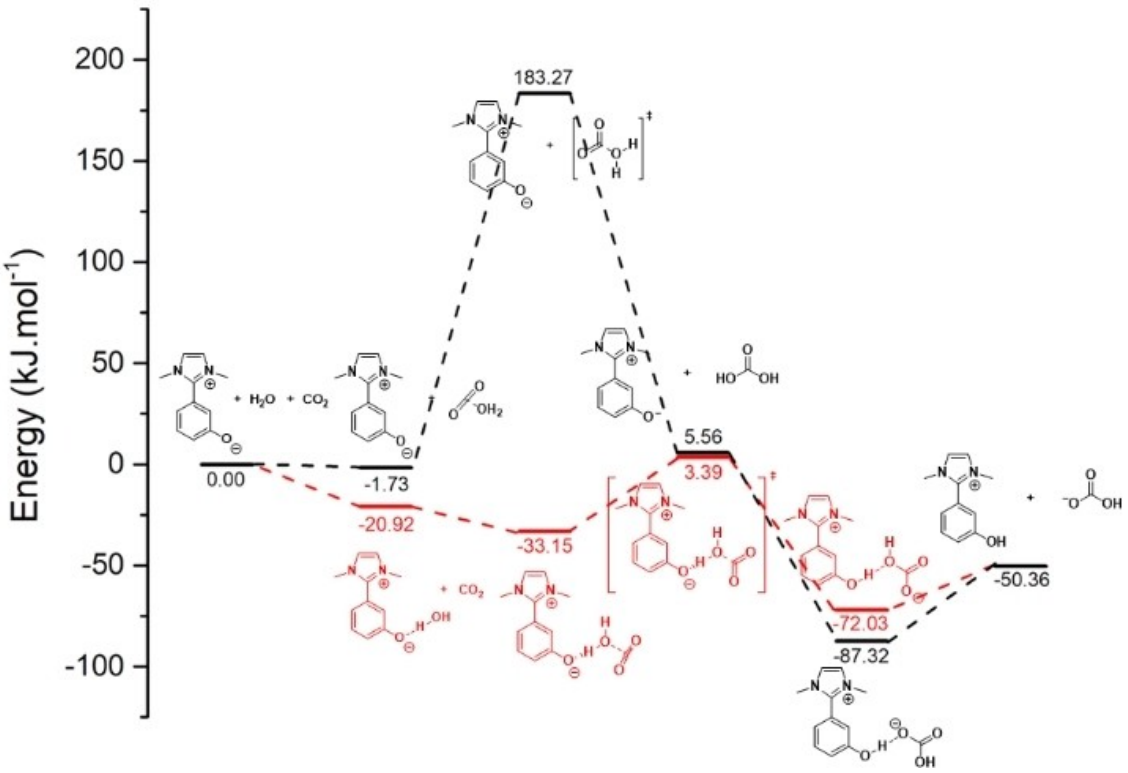

Scheme 2. Possible pathways involved in CO_2 sorption/desorption by aqueous solutions of **3**. Black Path I and red Path II.

found that the protonation occurs without an energy barrier indicating that carbonic acid is more acidic than **1**.

The energy-limiting step for Path I is the formation of carbonic acid from CO_2 and H_2O, with an activation energy of 185.00 kJ mol^{-1}.

Alternatively, in Path II, the solvated **3** approaches CO_2 molecule, followed by water nucleophilic attack to CO_2 and the proton is abstracted by **3** to form bicarbonate in a single step. The base acts as a water activator for CO_2 hydration, traditionally known as base-catalysed CO_2 hydration when sterically hindered amine solutions are used.[24] For **3**, the Path II exhibits a much lower energy barrier of 36.54 kJ mol^{-1} and is an exothermic reaction with a calculated △H value of −53.60 kJ mol^{-1}. The energy barrier for Path II is lower to the calculated activation energy for CO_2 absorption in aqueous MDEA solutions reported in the literature (40.9 kJ/mol,[14a] 38.5 kJ/mol[14b] and 42.43 kJ/mol.[25] According to Scheme 2, the Path I is unlikely because it has a higher energy barrier in the CO_2 hydration step, despite the carbonic acid deprotonating step being extremely favourable. The CO_2 capture by aqueous solutions of **3** is expected to occur via Path II (see Supporting Information, Figure S11 and Table S2 for more details). The cross-peak interaction between H_7 and H_{11} of the phenolate with HDO observed on NOESY results (Figure 3a) and the strong hydrogen bonds between the zwitterions and the surrounding water molecules calculated by DFT (Figure 5a) support our hypothesis of the mechanism via Path II. Here, we avoid using the term "base-catalyzed hydration" used by several authors and instead refer to the formation of a complex (**3** + H_2O) because the base is consumed in the process. The exact interactions involved in the formation of the complex (**3** + H_2O) is still unknown, but it may be related to contact ion pair reported in the literature by other authors in CO_2 capture processes in aqueous solutions of ionic liquids.[2d,26]

The recyclability of **3** and **4** for CO_2 absorption processes was confirmed by performing several sorption/desorption cycles. These cycles were compared with aqueous MDEA/piperazine aqueous solutions (Figure 7). Desorption was achieved by simply opening the reaction to room atmosphere and heating the solution to 100 °C. The aqueous solutions of **3** and **4** (1.0 M) exhibit at least the same chemisorption performance as the amine solution, considering reversibility and loading (total CO_2 absorbed/mole of sorbent). It is worth noting that CO_2 loading in the first cycle is greater than subsequent cycles for the solutions of **3** and **4**, especially **3**. This indicates that not all captured CO_2 was released under desorption conditions, which is consistent with the presence of residual bicarbonate observed after desorption in studies via ^{13}C NMR (as shown in Figure 6). The process of CO_2 sorption/desorption could be repeated at least 26 times without any significant changes in the performance from the second cycle, demonstrating the robustness of the system (Figure 7).

Inasmuch, the mechanism of CO_2 absorption by aqueous solutions of **3** is analogous to that of sterically hindered amine solutions, i.e., carbonate formation does not occur and the base acts as water activator for CO_2 hydration, the CO_2 desorption can be approximated by a single chemical equilibrium [Equation (7)]:[24]

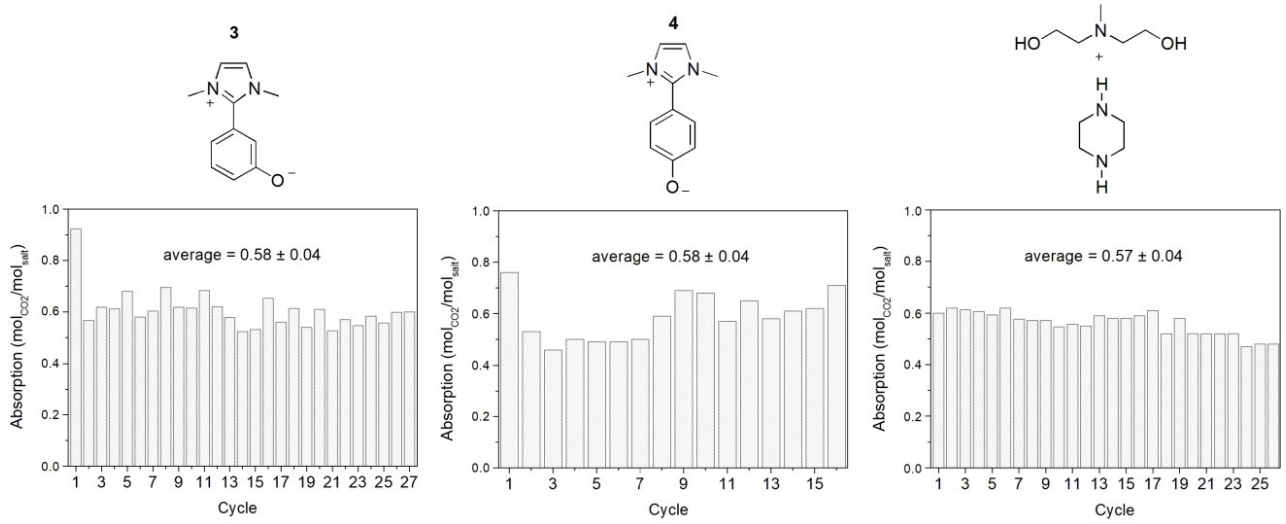

Figure 7. Performance of **3** and **4** aqueous solutions (1.0 M) in carbon dioxide sorption compared with MDEA/piperazine/H_2O (mass proportion 40:10:50) under the same experimental conditions (absorption at 1.3 bar of pure CO_2, 40 °C and desorption at 100 °C with a completely open vessel to the atmosphere) using an equilibrium chamber (Figure S12).

$$RPhOH_{(aq)} + HCO^-_{3(aq)} \rightleftharpoons RPhO^-_{(aq)} + CO_{2(aq)} + H_2O_{(l)} \quad (7)$$

The heat of reactions can be estimated from thermodynamics using the Gibbs-Helmholtz Equation (8):[27]

$$\left[\frac{\partial}{\partial T}\left(\frac{\Delta G}{T}\right)\right]_P = -\frac{\Delta H}{T^2} \quad (8)$$

As the equilibrium constant is not very affected by pressure, the relation between the temperature dependence of the equilibrium constant and heat of CO_2 desorption (ΔH_{des}) is given by Equation (9):[28]

$$\frac{d\left(\ln K''_{CO_2}\right)}{d\left(\frac{1}{T}\right)} = -\frac{\Delta H_{des}}{R} \quad (9)$$

The equilibrium constant (K''_{CO_2}) was determined at different temperatures ranging from 50 °C to 10 °C. Using the graphical method, and equation (9), the enthalpy of CO_2 desorption (ΔH_{des}) in solutions of **3** was estimated according to previously reported methodologies for MDEA.[29] The CO_2 absorption enthalpy ($\Delta H_{abs} = -\Delta H_{des}$) was estimated to be −38 kJ/mol, almost 30% lower than estimated for MDEA (−53.0 kJ/mol), which was used as a reference to validate the method under the same experimental conditions (Figure 8).

Hence, the aqueous solutions of **3** (1.0 M) reduce the desorption enthalpy when compared to the MDEA/H_2O system reported, which is usually around −49 kJ/mol.[29–30] This is an interesting aspect of this system, since the pKa of **3** is very close to the pKa of MDEA. There are some reasons for the lower estimated value of enthalpy for CO_2 desorption in aqueous solutions of **3** compared to MDEA (Figure 8) and the value calculated in Scheme 2. The desorption process involves the deprotonation of the conjugated acid of the applied base, and

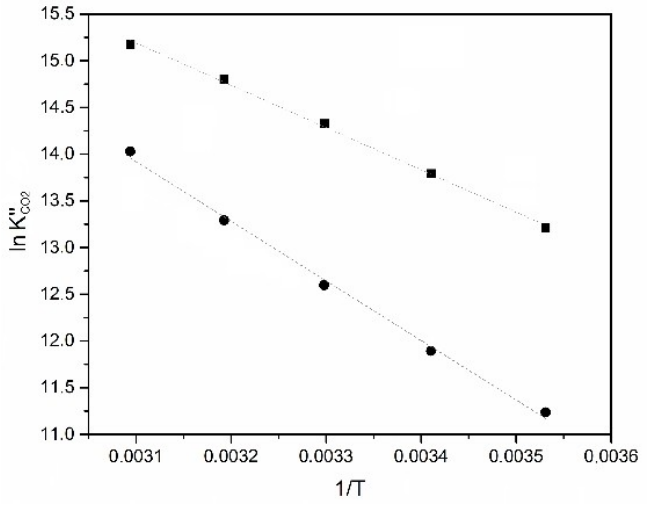

Figure 8. Plot of $\ln K''_{CO_2}$ *versus* $\left(1/T\right)$ for aqueous solutions of: ● MDEA (MDEA/H_2O mass proportion 30:70): ΔH_{abs} = −53 kJ/mol; and ■ zwitterion **3** (1.0 M): ΔH_{abs} = −38 kJ/mol, under the same experimental conditions (isochoric equilibrium chamber, 0.5 mL of solution between 10 and 50 °C).

the bond dissociation energy (BDE) of O–H bonds of phenols[31] differs from that of amino N–H bonds.[32] Additionally, to fully understand the thermodynamic origin of the enthalpy of desorption, the solvation enthalpies of the ionic species present in the media should be considered. The value of the solution enthalpy is determined by breaking solute-solute and solvent-solvent intermolecular interactions (endothermic terms) and forming solute-solvent interactions (exothermic term). It is well known that the solvation enthalpies of salts in water vary significantly with the anions[33] and cations.[34] In the case of zwitterionic compounds, the absorption process also involves neutralizing the charge of the phenolate group, which probably disrupt the structure of dimeric forms and reduce the net energy released. If so, the regeneration of dimeric forms during

the desorption step can provides extra energy to the system, reducing the enthalpy of desorption.

The relatively high intermolecular interaction of **3** is also reflected in the viscosity and density of concentrated aqueous solutions of **3** at 40 °C (3.5 M), which are slightly higher than MDEA solutions at the same concentration and temperature. Aqueous solutions of compound **4**, in which the intermolecular interactions are even stronger, have a density and viscosity greater than solutions of **3** at the same concentration and temperature (Figure S13). This may constitute some disadvantages in comparison with the MDEA systems, and its effects on the mass transfer phenomena of CO_2 capture processes will be published in a near future. Recent theoretical work indicates that phenoxides solutions exhibit a faster CO_2 hydration reaction kinetics compared to amine solutions.[35] However, a comprehensive assessment of the overall adsorption rate necessitates additional experimental data, including mass transfer information for CO_2 absorption in zwitterionic phenolate solutions. The obtained HP-^{13}C NMR data clearly show the ^{13}C signals of chemosorbed CO_2 are separated from those of physiosorbed CO_2. Therefore, it allows the estimation of Henry's solubility law[36] that was determined (without the interference of other CO_2 species that may be present in the aqueous solution),[37] by the quotient of the aqueous phase molality (m) to that of the gas phase and determined via inversed gated decoupling ^{13}C NMR analysis of the solutions with molality of 3.5 m (±0.1) at different pressures. The adsorption of CO_2 by aqueous solutions of **3** and **4** occurs mainly via the formation of bicarbonate at lower pressure. Physisorption becomes relevant with increasing pressure (>10 bar), similar to what was observed in the MDEA aqueous system (Figure 9). It is important to stress that only bicarbonate and physiosorbed CO_2 species were observed in all the high-pressure experiments and no decomposition of the zwitterionic moieties was detected by ^{13}C NMR. This represents a huge advantage of the basic aqueous zwitterionic solutions compared with other systems based on amines, carboxylates and phenolates reported so far that generally also generate CO_2 adducts.[23a,38]

The chemisorption of CO_2 (formation of bicarbonate) is almost constant (1.0 mol/mol; see Figure S8) from 10 to 40 bar, indicating that from 10 bar the base was completely consumed and the acid-base equilibrium is established. Only the amount of physiosorbed CO_2 increases with pressure (Figure 9). The total amount of chemo- and physiosorbed CO_2 of up to 1.3 mol/mol can be attained for aqueous solutions of **3** (3.5 molal) at 40 °C and 40 bar (Figure 9b).

The slope of the fitted curves for physiosorbed CO_2 data as a function of the pressure corresponds to Henry's solubility constant: 1.8×10^{-7}, 2.6×10^{-7} and 2.3×10^{-7} mol/kg/Pa for MDEA, **3** and **4**, respectively. Using Henry's solubility described in terms of molality has the advantage of remaining constant with temperature and highlighting the role of the solvent in physisorption. The obtained Henry's solubility coefficient for physiosorbed CO_2 is like that reported in bare water (2.33×10^{-7} mol/kg/Pa).[37c] Therefore, physisorption of the CO_2 in these aqueous systems is only slightly affected by the presence of basic sorbents. However, for practical purposes and better comparison with data in the literature, it is essential to conduct studies using traditional methodologies, such as the N_2O analogy, and this will be reported in the near future.

Conclusions

We have designed, prepared, and tested a new family of basic compounds that, in aqueous solutions, have the potential to replace the industrially employed aqueous amine solutions as CO_2 sorbents. The report data suggest that these zwitterionic compounds may offer several advantages. Firstly, the non-volatility of phenolate compounds **3** and **4** eliminates the costs associated with evaporation of the absorbent species. This potentially eliminates the need for the make-up step required in alkanolamines plants. Secondly, it was estimated a reduction of the desorption enthalpy with zwitterionic solutions by approximately 30% when compared to MDEA solutions. Additionally, the functional groups of the zwitterions are highly

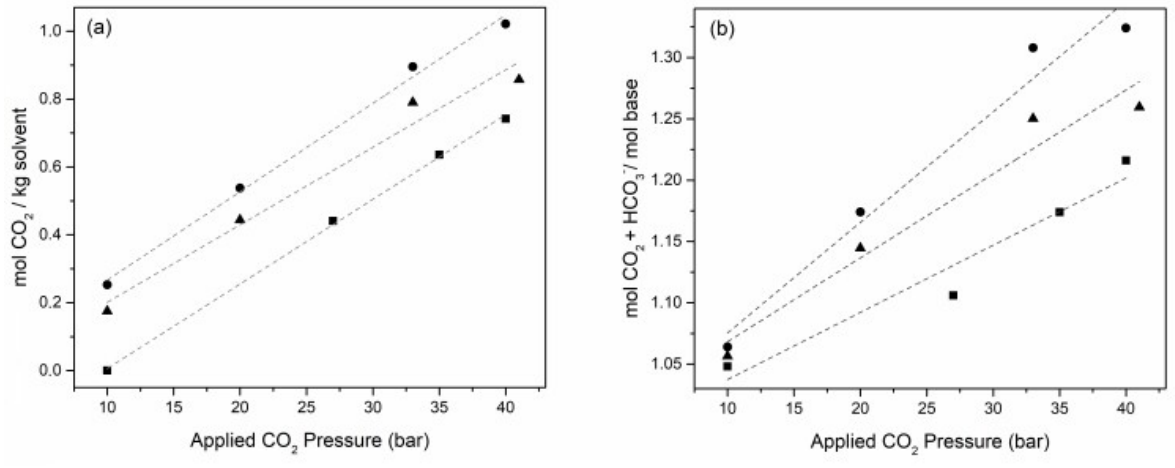

Figure 9. Physisorption (mol_{CO2}/kg_{solv}) (a) and chemo-plus physisorption (b) of CO_2 (mol/mol) by aqueous solutions (3.5 molal) of **3** (▲), **4** (●) and MDEA (■), **4** at different pressures (40 °C) determined by HP-^{13}C NMR using the integration of the bicarbonate peak (159.1 ppm).

robust, and the CO_2 capture is expected to occur via interaction of the complex (zwitterion + H_2O) and CO_2, with a calculated activation energy lower to that of CO_2 absorption in aqueous MDEA. These findings open new opportunities for studies related to kinetics, calorimetry, and selectivity of systems with zwitterionic bases, and for cost-effective CO_2 capture, activation, and functionalization.

In addition, environmental and safety advantages that are related to the non-volatility of the internal salts are presented, thus eliminating risks of possible human and environmental contamination. Finally, these new sorbents can replace CO_2/MDEA solutions in industrial plants with little or no modifications.

Experimental Section

General

All reactions were performed in air and all reagents were from commercial sources. N-methyl-diethanolamine (MDEA; ≥99%), 3-hydroxy-benzaldehyde (≥99%), 4-hydroxy-benzaldehyde (98%), iodomethane (CH_3I; ≥99%), ammonium carbonate (≥30% NH_3 basis) and piperazine (99%) were obtained from Sigma-Aldrich Merck (Germany) and were used as received. The industrial mixture of the aqueous MDEA/piperazine solution was provided by PETROBRAS. Commercial compounds were used without further purification. Thermogravimetric analysis (TGA) was performed using a TA Q50 calorimeter. Differential scanning calorimetry (DSC) analyses were performed in a DSC Q2000 (TA Instruments). All NMR experiments were conducted using a Bruker Avance-IIIHD 400 spectrometer equipped with a BBO 5 mm probe with z-gradients operating at 400.06 MHz for ^1H and 100.46 MHz for ^{13}C. Spectra were obtained at 298 K under typical conditions for ^1H (spectral width 6400 Hz with 32 k data points and zero-filled to 128 k to give a digital resolution of 0.05 Hz per pt). The 2D-NOESY experiment used a pre-scan delay of 2.0 s, 1024 F1 increments and 4096 data points in the acquisition dimension. Data were processed using zero-filling up to 1024 and the qsine window was applied in both the F1 and F2 dimensions, prior to Fourier transformation to give an FID resolution of 1.5 Hz. The high-pressure (HP-^{13}C NMR) inverse gated decoupling experiments were carried out using a Bruker Avance-IIIHD 400 spectrometer equipped with a BBO 5 mm probe with z-gradients operating at 400.06 MHz for ^1H and 100.46 MHz for ^{13}C and a Daedalus Xtreme 60 pump using a 5 mm (3.6 mm) zirconia NMR tube. The solutions of salts **3** and **4** were prepared in water as a solvent. The HP-^{13}C NMR experiments with different CO_2 pressures were done after stabilization (8 h) at a temperature of 40 °C. Spectra were obtained at 40 °C under conditions for HP-^{13}C NMR (spectral width 8012 Hz with 32 k data points and zero-filled to 64 k to give an FID resolution of 0.48 Hz, d1 40 s and NS 1024) (Figure S9). Ultraviolet–visible spectroscopy (UV-vis) experiments were performed using a Shimadzu 2450 spectrophotometer. The viscosity and density of aqueous solutions of **3** and **4** were determined in Anton Paar SVM 3000 apparatus between 40 and 100 °C.

Preparation of 1-methyl-2-(3-hydroxyphenyl) imidazole

The synthesis was performed as a multicomponent 'one pot' reaction. Firstly, methylamine (40% aqueous solution, 16.50 g; 210 mmol) was added to 3-hydroxy-benzaldehyde solution (24.40 g; 200 mmol, dissolved in 150 mL of methanol). The resulting amber solution was stirred for another 10 min. In the next step, ammonium carbonate (14.40 g; 150 mmol) was added at once and then the glyoxal solution (40% aqueous solution, 29.00 g; 200 mmol, dissolved in 30 mL of methanol) was added dropwise under vigorous stirring, maintaining the reaction mixture at room temperature. Carbon dioxide evolved during this last addition and the desired imidazole precipitated. Afterwards, the reaction mixture was stirred for about 90 min. After this time, 250 mL of ice water was added to the reaction flask, then the crystals were filtered with a Büchner funnel and washed with a 1:2 mixture of ice-cold methanol/water. The obtained pale amber crystals were dried under reduced pressure. Yield: 36.8%; 12.80 g. ^1H NMR (400 MHz, DMSO-d_6) δ 9.68 (br s, 1H), 7.26 (t, 8 Hz, 1H), 7.21 (s, 1H), 7.15–7.05 (m, 2H), 6.96 (s, 1H), 6.85–6.80 (m, 1H), 3.71 (s, 3H). ^{13}C NMR (100 MHz, DMSO-d_6) δ 157.42, 146.56, 131.89, 129.51, 127.44, 123.31, 118.85, 115.40, 115.20, 34.38.

Preparation of 1,3-dimethyl-2-(3-hydroxyphenyl) imidazolium iodide (1)

1-Methyl-2-(3-hydroxyphenyl) imidazole (14.80 g; 85.0 mmol) was placed in a 500 mL round-bottomed flask provided with a reflux condenser and addition funnel. Acetonitrile (100 mL) was added to the flask and CH_3I (15.00 g; 105.6 mmol, dissolved in 10 mL) was added dropwise from the addition funnel for 45 min, maintaining the reaction mixture at 70 °C under stirring. Cold water was circulated in the reflux condenser to ensure trapping of the CH_3I. The reacting imidazole was slightly soluble in acetonitrile but reacted in solution at 70 °C. After stirring for another 2 h, the resulting solution was concentrated to 20 mL and ethyl acetate (50 mL) was added to precipitate most of the product. The resulting pale, amber-coloured crystals were filtered with a Büchner funnel, washed with ethyl acetate and dried under reduced pressure. Yield: 92.3%; 24.80 g. ^1H NMR (400 MHz, D_2O) δ 7.55 (t, 1H), 7.52 (s, 2H), 7.21–7.18 (m, 1H), 7.14 (m, 1H), 7.09–7.08 (m, 1H), 3.71 (s, 6H). ^{13}C NMR (101 MHz, D_2O) δ 156.32, 144.39, 131.08, 122.80, 122.13, 122.09, 119.46, 116.86, 35.51.

Preparation of synthesis of 1,3-dimethyl-2-(3-oxyphenyl) imidazolium zwitterion (3)

AmberSep 900 OH ion exchange resin (14 mL, 0.8 meq OH^-/mL, 11.2 meq OH^-) was placed in a 50 mL beaker and was washed three times with distilled water. 1,3-Dimethyl-2-(3-hydroxyphenyl) imidazolium iodide solution (3.164 g; 10.00 mmol, dissolved in 10 mL of water) was added to the resin and the resulting suspension was stirred at room temperature for 20 min. The I^-/OH^- exchange was confirmed by performing a negative qualitative iodide test (nitrite/sulphuric acid). The solution was filtered with a Büchner funnel, and the water was evaporated under reduced pressure, resulting in a yellowish-white solid. Yield: 96.0%, 1.810 g. ^1H NMR (400 MHz, D_2O) δ 7.40 (s, 2H), 7.33–7.27 (m, 1H), 6.84 (dd, J = 8.0, 2.7 Hz, 1H), 6.66–6.58 (m, 2H), 3.64 (s, 6H). ^{13}C NMR (101 MHz, D_2O) δ 166.97, 145.76, 130.47, 122.66, 122.24, 121.95, 119.51, 115.07, 35.15.

Preparation of 1-methyl-2-(4-hydroxyphenyl) imidazole

This synthesis was performed as a multicomponent 'one pot' reaction. Firstly, methylamine (40% aqueous solution, 81.4 g; 1050 mmol) was added over 4-hydroxy-benzaldehyde solution (122 g; 1000 mmol, dissolved in 350 mL of methanol). The reaction heats up to about 40 °C. The resulting amber solution was stirred for another 10 min. In the next step, ammonium carbonate (72 g; 750 mmol) was added at once and then the glyoxal solution (40% aqueous solution, 145 g; 1000 mmol, dissolved in 150 mL of

methanol) was added dropwise under vigorous stirring, maintaining the temperature of the reaction mixture between 40 and 45 °C. Carbon dioxide evolved during this last addition and the desired imidazole precipitated. After the addition, the reaction mixture was stirred for about 90 min. After this time, 500 mL of ice water was added to the reaction flask, the crystals were filtered with a Büchner funnel and washed with a 1 : 2 mixture of ice-cold methanol/water. The obtained pale amber crystals were dried under reduced pressure. Yield: 49.5 %; 86.2 g. ^{1}H NMR (400 MHz, DMSO-d_6) δ 9.90 (s, 1H), 7.48 (d, J = 8.8 Hz, 2H), 7.17 (d, J = 1.2 Hz, 1H), 6.91 (d, J = 1.2 Hz, 1H), 6.85 (d, J = 8.8 Hz, 2H), 3.68 (s, 3H). ^{13}C NMR (101 MHz, DMSO-d_6) δ 157.68, 146.93, 129.73, 127.10, 122.62, 121.60, 115.25, 34.20.

Preparation of 1,3-dimethyl-2-(4-hydroxyphenyl) imidazolium iodide (2)

1-Methyl-2-(4-hydroxyphenyl) imidazole (86.2 g; 495 mmol) was placed in a 2 L round-bottomed flask provided with a reflux condenser and addition funnel. Acetonitrile (550 mL) was added to the flask and CH_3I (85 g; 594 mmol, dissolved in 50 mL) was added dropwise from the addition funnel for 45 min, maintaining the reaction mixture at 70 °C under stirring. Cold water was circulated in the reflux condenser to ensure trapping of the CH_3I. The reacting imidazole was slightly soluble in acetonitrile, but reacted in solution at 70 °C, and the resulting imidazolium salt, also slightly soluble in acetonitrile, precipitated. After stirring for another 2 h, 600 mL of ethyl acetate was added to precipitate most of the product. The resulting straw-coloured crystals were filtered with a Büchner funnel, washed with ethyl acetate and dried under reduced pressure. Yield: 95 %; 149.6 g. ^{1}H NMR (400 MHz, DMSO-d_6) δ 10.41 (s, 1H), 7.84 (s, 2H), 7.58 (d, J = 8.9 Hz, 2H), 7.01 (d, J = 8.9 Hz, 2H), 3.68 (s, 6H). ^{13}C NMR (101 MHz, DMSO-d_6) δ 160.62, 144.59, 132.37, 122.80, 116.10, 110.96, 35.73.

Preparation of 1,3-dimethyl-2-(4-oxyphenyl) imidazolium zwitterion (4)

AmberSep 900 OH ion exchange resin (700 mL, 0.8 meq OH^-/mL, 560 meq OH^-) was placed in a 2 L beaker and was washed three times with distilled water. 1,3-Dimethyl-2-(4-hydroxyphenyl) imidazolium iodide solution (158.2 g; 500 mmol, dissolved in 500 mL of water) was added to the resin and the resulting suspension was stirred at room temperature for 60 min. The I^-/OH^- exchange was confirmed by performing a negative qualitative iodide test (nitrite/sulphuric acid). The solution was filtered with a Büchner funnel, and the water was evaporated under reduced pressure, resulting in a yellowish-white solid. Yield: 82.2 %, 77.3 g. ^{1}H NMR (400 MHz, DMSO-d_6) δ 7.60 (s, 2H), 7.00 (d, J = 8.8 Hz, 2H), 6.16 (d, J = 8.8 Hz, 2H), 3.67 (s, 6H). ^{13}C NMR (100 MHz, H_2O with DMSO-d_6 internal capillary tube) δ 168.70, 145.13, 130.21, 121.13, 118.17, 104.25, 34.22.

X-ray structure of 3 and 4

A Bruker D8 Venture Photon 100 dual source diffractometer was used to collect X-ray data for the structural analysis. Data were collected using Mo–Kα radiation, and a combination of ϕ and ω scans was carried out to obtain at least one unique data set. The structures were solved using direct methods with SHELXS.[39] The final structures were refined using SHELXL,[39] where the remaining atoms were located from difference Fourier synthesis. Anisotropic displacement parameters were applied to all non-hydrogen atoms followed by full-matrix least-squares refinement based on F2. All hydrogen atoms were placed in ideal positions and refined as riding atoms with relative isotropic displacement parameters, except that hydrogen linked to the oxygen atoms was introduced in the structural model through Fourier difference maps analysis.

Deposition Numbers 2195923 (for **3**) and 2195924 (for **4**) contains the supplementary crystallographic data for this paper. These data are provided free of charge by the joint Cambridge Crystallographic Data Centre and Fachinformationszentrum Karlsruhe Access Structures service.

Quantum mechanical calculations

Quantum mechanical calculations aiming to predict the pKa values of the phenolic substitutions were carried out with Gaussian 16 software, Revision A.03.[40] Following the procedure outlined in a QSPR study focusing on the pKa of phenols,[41] we computed the Mulliken charges at the HF//6-31G* level of theory for several imidazolium cations carrying the phenolic substitution at C2. This level of theory combined with Mulliken charges has been highlighted to furnish the best correlation between predicted and experimental pKa values of phenolic substances.[41] Within this QSPR approach, the Mulliken charges of the carbon atom connected to the hydroxyl substitution, as well as the charges of the OH group, represent the only parameters in the pKa prediction. All structural calculations were also performed with the program Gaussian 16, Revision A.03 at the DFT level wB97XD/6-311++G(2d,p) and using water as the implicit solvent through the polarizable continuum model (PCM-SMD). All structures were full optimized to a minimum of energy and confirmed through vibrational analysis where no imaginary frequencies were obtained. The transition states found were confirmed by vibrational analysis as well, containing one, and only one, imaginary frequency mode relevant to the reaction. To assure that the methodology used was accurate, results obtained for CO2 absorption with MDEA and H2O at wB97XD/6-311++G(2d,p) level of theory using water as the implicit solvent (PCM-SMD) were compared with data found in the literature (Supporting Information). The analysis of the results was performed using the software Chemcraft (http://www.chemcraftprog.com/) and Mercury.[42]

Simulation of CO_2 sorption as function of pKa

The main equilibrium equations involved in CO_2 capture by generic basic aqueous solutions and simulations are presented in the Supporting Information.

Acid dissociation constant (pKa) determination

Potentiometric measurements were conducted with a Bench Type HI 2210 pH meter with an HI 1131B pH electrode, glass body, single junction (uncertainty ±0.01 pH) and HI 7662 temperature sensor (uncertainty ±0.1 °C). The temperature was controlled at 25 °C with a Huber heating circulator (temperature stability ±0.1 °C). Deionized water was used as the heat transfer medium. Calibration of the pH electrode was performed using buffer solutions traceable to the National Bureau of Standards (pH 4.01, 9.21 and 10.26).[43] Methyl ethanol amine (MEA) was used as a reference compound to validate the calibration. The MEA conjugated acid gave a pKa value of 9.50, which agrees well with literature values varying between 9.44 and 9.508.[43–44] Aqueous zwitterionic solutions (10 mL, 0.1 M) were titrated with 0.1 M HCl solution. All measurements were performed in duplicate, and the average values are reported. Average deviations of the duplicates were < 1%. Aliquots of 0.2 mL of titrant were added and the pH was recorded. pKa values were calculated as the pH at half equivalence as presented in Figure S1.

CO_2 absorption/desorption capacity experiments

The CO_2 sorption and desorption tests were carried out in apparatus that keeps the temperature and pressure of the sorption vessel constant and monitors the pressure drop in a CO_2 reservoir, allowing determination of the amount of gas sorbed. A depiction of the apparatus and set-up is given in Figure S12. The pressure control valve was adjusted to maintain the pressure of the sorption vessel at 1.3 bar absolute during the absorption test. The temperature of the reaction vessel was adjusted to the absorption temperature (T1), typically 40 °C. Then, 5 mL of 1 M aqueous salt of 1,3-dimethyl-2-(3-oxy-phenyl)-imidazolium or 1,3-dimethyl-2-(4-oxy-phenyl)-imidazolium was added to the reaction vessel. The system was purged with CO_2 for 5 s, closed and the reservoir filled with CO_2 at 4 bar (absolute). The magnetic stirrer was initiated, and the pressure drop in the CO_2 reservoir monitored to determine the number of moles of CO_2 consumed. For the calculations, the ideal gas state equation and the previously calibrated volume of the reservoir were considered. The end point of absorption was determined when a plateau was observed for at least 10 min on the reservoir pressure graph as a function of time. At the end of the absorption stage, the system was opened, and the temperature of the thermostatic bath adjusted to the desorption temperature (T2), typically 100 °C. The system was kept under agitation for 30 min for regeneration of the zwitterionic solution.

Estimation of enthalpy of absorption of CO_2

The enthalpy of absorption in internal salt **3** aqueous solutions was estimated for

(0.5 mL, 1 M) using the similar methodology reported by Gabrielsen and collaborators to estimate the heat of CO_2 absorption by aqueous solutions of alkanolamines.[29] To validate the method, a mixture of MDEA/water (mass proportion 30:70) was used as reference.

Viscosity measurements

Variation of the kinematic viscosity of the aqueous solutions (3.5 M) of **3**, **4** and MDEA/piperazine/water (40/10/50) with temperature was determined between 40 and 100 °C (see Figure S13). The kinematic viscosity increased from 4.7462 mm^2/s for MDEA/piperazine to 5.9225 mm^2/s at 40 °C.

Density measurements

Variation of the density of the aqueous solutions (3.5 M) of **3**, **4** and MDEA/piperazine/water (40/10/50) with temperature was determined between 40 and 100 °C (see Figure S13).

Henry low constant

Aqueous solutions of sorbent agent with molality of 3.5 m were introduced into a 5 mm (3.6 mm) zirconia NMR tube and pressurized with CO_2 using a Daedalus Xtreme 60 pump. For each analysis, the pressure and temperature were kept constant for 12 h so that equilibrium was reached, and the HP-^{13}C NMR was used to quantify the dissolved gas.

Supporting Information

The authors have cited additional references within the Supporting Information (Ref. [45]).

Acknowledgements

We are grateful to CAPES (001), FAPERGS (22/2551-0000386-9), CNPq (406260/2018-4) and PETROBRAS (SAP4600579154) for financial support.

Conflict of Interests

The authors declare the following competing financial interest(s): There has been filed a patent application with the following information: Applicant: Petróleo Brasileiro S.A. - PETROBRAS Name of inventors: do Nascimento, J. F., Dupont, J., de Menezes, S. C., dos Santos F. P., Marin, G., de Lemos, G. A. P., Ebeling, G. Application number: BR1020200270710 and PCT/BR2021/050557. Status of application: Filed Specific aspect of manuscript covered in patent application: Synthesis process of zwitterionic bases, CO_2 capture process and use.

Data Availability Statement

The data that support the findings of this study are available from the corresponding author upon reasonable request.

Keywords: carbon dioxide capture · ionic liquids · organic base · zwitterion · bicarbonate

[1] a) J. E. Bara, D. E. Camper, D. L. Gin, R. D. Noble, *Acc. Chem. Res.* **2010**, *43*, 152–159; b) P. Madejski, K. Chmiel, N. Subramanian, T. Kuś, *Energies* **2022**, *15*, 887–908; c) Z. Cheng, S. Li, Y. Liu, Y. Zhang, Z. Ling, M. Yang, L. Jiang, Y. Song, *Renewable Sustainable Energy Rev.* **2022**, *154*, AN111806; d) B. Smit, A.-H. A. Park, G. Gadikota, *Front. Energy Res.* **2014**, *2*, DOI: 10.3389/fenrg.2014.00055; e) B. P. Spigarelli, S. K. Kawatra, *J. CO2 Util.* **2013**, *1*, 69–87.
[2] a) P. Panja, B. McPherson, M. Deo, *Carbon Capture Sci. Technol.* **2022**, *3*, AN100041; b) F. Hussin, M. K. Aroua, *J. Cleaner Prod.* **2020**, *253*, e119707; c) F. O. Ochedi, J. Yu, H. Yu, Y. Liu, A. Hussain, *Environ. Chem. Lett.* **2020**, *19*, 77–109; d) J. Dupont, N. M. Simon, M. Zanatta, F. P. Dos Santos, M. C. Corvo, E. J. Cabrita, *ChemSusChem* **2017**, *10*, 4927–4933; e) C. E. Wilmer, O. K. Farha, Y.-S. Bae, J. T. Hupp, R. Q. Snurr, *Energy Environ. Sci.* **2012**, *5*, 9849–9856.
[3] a) J. K. Stolaroff, D. W. Keith, G. V. Lowry, *Environ. Sci. Technol.* **2008**, *42*, 2728–2735; b) Y. E. Kim, J. A. Lim, S. K. Jeong, Y. I. Yoon, S. T. Bae, S. C. Nam, *Bull. Korean Chem. Soc.* **2013**, *34*, 783–787.
[4] R. Shao, A. Stangeland, *The Bellona Foundation* **2009**, 1–49.
[5] a) M. T. Mota-Martinez, P. Brandl, J. P. Hallett, N. Mac Dowell, *Mol. Syst. Des. Eng.* **2018**, *3*, 560–571; b) X. P. Zhang, X. C. Zhang, H. F. Dong, Z. J. Zhao, S. J. Zhang, Y. Huang, *Energy Environ. Sci.* **2012**, *5*, 6668–6681; c) J. F. Brennecke, B. E. Gurkan, *J. Phys. Chem. Lett.* **2010**, *1*, 3459–3464; d) G. Cui, J. Wang, S. Zhang, *Chem. Soc. Rev.* **2016**, *45*, 4307–4339.
[6] a) S. Zeng, X. Zhang, L. Bai, X. Zhang, H. Wang, J. Wang, D. Bao, M. Li, X. Liu, S. Zhang, *Chem. Rev.* **2017**, *117*, 9625–9673; b) S. K. Shukla, S. G. Khokarale, T. Q. Bui, J.-P. T. Mikkola, *Front. Mater.* **2019**, *6*, DOI: 10.3389/fmats.2019.00042.
[7] a) M. J. Earle, J. M. Esperanca, M. A. Gilea, J. N. Lopes, L. P. Rebelo, J. W. Magee, K. R. Seddon, J. A. Widegren, *Nature* **2006**, *439*, 831–834; b) M. A.

Rocha, C. F. Lima, L. R. Gomes, B. Schroder, J. A. Coutinho, I. M. Marrucho, J. M. Esperanca, L. P. Rebelo, K. Shimizu, J. N. Lopes, L. M. Santos, *J. Phys. Chem. B* **2011**, *115*, 10919–10926.
[8] L. I. Helgesen, E. Gjernes, *Energy Procedia* **2016**, *86*, 239–251.
[9] P. J. Carvalho, K. A. Kurnia, J. A. Coutinho, *Phys. Chem. Chem. Phys.* **2016**, *18*, 14757–14771.
[10] E. D. Bates, R. D. Mayton, I. Ntai, J. H. Davis Jr., *J. Am. Chem. Soc.* **2002**, *124*, 926–927.
[11] a) M. Zanatta, N. M. Simon, F. P. Dos Santos, M. C. Corvo, E. J. Cabrita, J. Dupont, *Angew. Chem. Int. Ed. Engl.* **2019**, *58*, 382–385; b) J. Dupont, N. Simon, M. Zanatta, *ChemSusChem* **2020**, *13*, 1817; c) T. B. Lee, S. Oh, T. R. Gohndrone, O. Morales-Collazo, S. Seo, J. F. Brennecke, W. F. Schneider, *J. Phys. Chem. B* **2016**, *120*, 1509–1517; d) M. Besnard, M. I. Cabaco, F. V. Chavez, N. Pinaud, P. J. Sebastiao, J. A. Coutinho, Y. Danten, *Chem. Commun.* **2012**, *48*, 1245–1247; e) G. Gurau, H. Rodriguez, S. P. Kelley, P. Janiczek, R. S. Kalb, R. D. Rogers, *Angew. Chem. Int. Ed. Engl.* **2011**, *50*, 12024–12026; f) C. Wang, X. Luo, H. Luo, D.-e. Jiang, H. Li, S. Dai, *Angew. Chem. Int. Ed.* **2011**, *50*, 4918–4922; g) D.-J. Tao, F.-F. Chen, Z.-Q. Tian, K. Huang, S. M. Mahurin, D.-e. Jiang, S. Dai, *Angew. Chem. Int. Ed.* **2017**, *56*, 6843–6847; h) Y. Huang, G. Cui, Y. Zhao, H. Wang, Z. Li, S. Dai, J. Wang, *Angew. Chem. Int. Ed. Engl.* **2017**, *56*, 13293–13297; i) F. F. Chen, K. Huang, Y. Zhou, Z. Q. Tian, X. Zhu, D. J. Tao, D. E. Jiang, S. Dai, *Angew. Chem. Int. Ed. Engl.* **2016**, *55*, 7166–7170; j) X. Luo, Y. Guo, F. Ding, H. Zhao, G. Cui, H. Li, C. Wang, *Angew. Chem. Int. Ed. Engl.* **2014**, *53*, 7053–7057; k) T. Oncsik, R. Vijayaraghavan, D. R. MacFarlane, *Chem. Commun.* **2018**, *54*, 2106–2109; l) D. Hospital-Benito, J. Lemus, C. Moya, R. Santiago, J. Palomar, *Chem. Eng. J. Adv.* **2022**, *10*, 100291.
[12] J. F. do Nascimento, J. Dupont, S. M. C. de Menezes, F. P. dos Santos, G. Marin, G. L. Aydos, G. Ebeling, (Ed.: PCT/BR2021/050557), UFRGS and PETROBRAS, Brazil, **2021**.
[13] P. Pakzad, M. Mofarahi, M. Ansarpour, M. Afkhamipour, C.-H. Lee, in *Advances in Carbon Capture* (Eds.: M. R. Rahimpour, M. Farsi, M. A. Makarem), Woodhead Publishing, **2020**, pp. 51–87.
[14] a) M. Narimani, S. Amjad-Iranagh, H. Modarress, *J. Nat. Gas Sci. Eng.* **2017**, *47*, 154–166; b) W.-C. Yu, G. Astarita, D. W. Savage, *Chem. Eng. Sci.* **1985**, *40*, 1585–1590.
[15] a) K. G. Joback, J. R. Heberle, A. S. Bhown, *Energy Procedia* **2017**, *114*, 1689–1708; b) E. F. da Silva, H. F. Svendsen, *Int. J. Greenhouse Gas Control* **2007**, *1*, 151–157.
[16] a) D. Pines, J. Ditkovich, T. Mukra, Y. Miller, P. M. Kiefer, S. Daschakraborty, J. T. Hynes, E. Pines, *J. Phys. Chem. B* **2016**, *120*, 2440–2451; b) T. Loerting, J. Bernard, *ChemPhysChem* **2010**, *11*, 2305–2309.
[17] J. E. Wheatley, S. Bala, D. C. Barnes, C. Schoolderman, G. Jakab, G. Raynel, C. M. Rayner, *Int. J. Greenhouse Gas Control* **2019**, *88*, 353–360.
[18] J. Catalá, M. P. Caballero, F. de la Cruz-Martínez, J. Tejeda, J. A. Castro-Osma, A. Lara-Sánchez, J. M. García-Vargas, M. T. García, M. J. Ramos, I. Gracia, J. F. Rodríguez, *J. CO2 Util.* **2022**, *61*, 102060.
[19] G. M. Battle, G. M. Ferrence, F. H. Allen, *J. Appl. Crystallogr.* **2010**, *43*, 1208–1223.
[20] C. R. Martinez, B. L. Iverson, *Chem. Sci.* **2012**, *3*, 2191–2201.
[21] a) N. M. Simon, M. Zanatta, J. Neumann, A. L. Girard, G. Marin, H. Stassen, J. Dupont, *ChemPhysChem* **2018**, *19*, 2879–2884; b) H. K. Stassen, R. Ludwig, A. Wulf, J. Dupont, *Chem. Eur. J.* **2015**, *21*, 8324–8335.
[22] J. C. Dearden, W. F. Forbes, *Can. J. Chem.* **1959**, *37*, 1294–1304.
[23] a) C. Wang, H. Luo, D. E. Jiang, H. Li, S. Dai, *Angew. Chem. Int. Ed. Engl.* **2010**, *49*, 5978–5981; b) C. Wang, X. Luo, H. Luo, D. E. Jiang, H. Li, S. Dai, *Angew. Chem. Int. Ed. Engl.* **2011**, *50*, 4918–4922.
[24] T. L. Donaldson, Y. N. Nguyen, *Ind. Eng. Chem. Fundam.* **1980**, *19*, 260–266.
[25] G. F. Versteeg, W. P. M. van Swaaij, *Chem. Eng. Sci.* **1988**, *43*, 587–591.
[26] M. Zanatta, A. L. Girard, G. Marin, G. Ebeling, F. P. Dos Santos, C. Valsecchi, H. Stassen, P. R. Livotto, W. Lewis, J. Dupont, *Phys. Chem. Chem. Phys.* **2016**, *18*, 18297–18304.
[27] J. B. Ott, J. Boerio-Goates, in *Chemical Thermodynamics: Principles and Applications* (Eds.: J. B. Ott, J. Boerio-Goates), Academic Press, London, **2000**, pp. 105–153.
[28] A. E. Sherwood, J. M. Prausnitz, *AlChE J.* **1962**, *8*, 519–521.
[29] J. Gabrielsen, M. L. Michelsen, E. H. Stenby, G. M. Kontogeorgis, *Ind. Eng. Chem. Res.* **2005**, *44*, 3348–3354.
[30] J. K. Carson, K. N. Marsh, A. E. Mather, *J. Chem. Thermodyn.* **2000**, *32*, 1285–1296.
[31] O. V. Dorofeeva, O. N. Ryzhova, *J. Phys. Chem. A* **2016**, *120*, 2471–2479.
[32] J. Lalevee, X. Allonas, J. P. Fouassier, *J. Am. Chem. Soc.* **2002**, *124*, 9613–9621.
[33] M. A. Varfolomeev, A. A. Khachatrian, B. S. Akhmadeev, B. N. Solomonov, A. V. Yermalayeu, S. P. Verevkin, *J. Solution Chem.* **2015**, *44*, 811–823.
[34] C. V. Krishnan, H. L. Friedman, *J. Phys. Chem.* **2002**, *73*, 3934–3940.
[35] Z. Zhang, A. L. Kummeth, J. Y. Yang, A. N. Alexandrova, *Proc. Natl. Acad. Sci. USA* **2022**, *119*, e2123496119.
[36] a) R. Sander, W. E. Acree, A. De Visscher, S. E. Schwartz, T. J. Wallington, *Pure Appl. Chem.* **2022**, *94*, 71–85; b) R. Sander, *Atmos. Chem. Phys.* **2015**, *15*, 4399–4981.
[37] a) G. W. Xu, C. F. Zhang, S. J. Qin, W. H. Gao, H. B. Liu, *Ind. Eng. Chem. Res.* **1998**, *37*, 1473–1477; b) L. Li, M. Maeder, R. Burns, G. Puxty, S. Clifford, H. Yu, *Energy Procedia* **2017**, *114*, 1841–1847; c) E. Skylogianni, C. Perinu, B. Y. C. Gameros, H. K. Knuutila, *J. Chem. Thermodyn.* **2020**, *151*, AN106176.
[38] S. F. R. Taylor, C. McCrellis, C. McStay, J. Jacquemin, C. Hardacre, M. Mercy, R. G. Bell, N. H. de Leeuw, *J. Solution Chem.* **2015**, *44*, 511–527.
[39] G. M. Sheldrick, *Acta Crystallogr. Sect. A* **2008**, *64*, 112–122.
[40] M. J. Frisch, G. W. Trucks, H. B. Schlegel, G. E. Scuseria, M. A. Robb, J. R. Cheeseman, G. Scalmani, V. Barone, G. A. Petersson, H. Nakatsuji, X. Li, M. Caricato, A. V. Marenich, J. Bloino, B. G. Janesko, R. Gomperts, B. Mennucci, H. P. Hratchian, J. V. Ortiz, A. F. Izmaylov, J. L. Sonnenberg, Williams, F. Ding, F. Lipparini, F. Egidi, J. Goings, B. Peng, A. Petrone, T. Henderson, D. Ranasinghe, V. G. Zakrzewski, J. Gao, N. Rega, G. Zheng, W. Liang, M. Hada, M. Ehara, K. Toyota, R. Fukuda, J. Hasegawa, M. Ishida, T. Nakajima, Y. Honda, O. Kitao, H. Nakai, T. Vreven, K. Throssell, J. A. Montgomery Jr., J. E. Peralta, F. Ogliaro, M. J. Bearpark, J. J. Heyd, E. N. Brothers, K. N. Kudin, V. N. Staroverov, T. A. Keith, R. Kobayashi, J. Normand, K. Raghavachari, A. P. Rendell, J. C. Burant, S. S. Iyengar, J. Tomasi, M. Cossi, J. M. Millam, M. Klene, C. Adamo, R. Cammi, J. W. Ochterski, R. L. Martin, K. Morokuma, O. Farkas, J. B. Foresman, D. J. Fox, *Gaussian 16 Rev. C.01*, Wallingford, CT, **2016**.
[41] A. C. Lee, G. M. Crippen, *J. Chem. Inf. Model.* **2009**, *49*, 2013–2033.
[42] C. F. Macrae, I. Sovago, S. J. Cottrell, P. T. A. Galek, P. McCabe, E. Pidcock, M. Platings, G. P. Shields, J. S. Stevens, M. Towler, P. A. Wood, *J. Appl. Crystallogr.* **2020**, *53*, 226–235.
[43] R. G. Bates, G. D. Pinching, *J. Res. Natl. Bur. Stand.* **1951**, *46*, 349–352.
[44] a) A. Hartono, M. Saeed, I. Kim, H. F. Svendsen, *Energy Procedia* **2014**, *63*, 1122–1128; b) S. Evjen, I. R. Krokvik, A. Fiksahl, H. Knuutila, *Energy Procedia* **2017**, *114*, 2590–2598.
[45] a) J.-J. Ko, M.-H. Li, *Chem. Eng. Sci.* **2000**, *55*, 4139–4147; b) C. Mathonat, V. Majer, A. E. Mather, J. P. E. Grolier, *Fluid Phase Equilib.* **1997**, *140*, 171–182.

Manuscript received: July 6, 2023
Revised manuscript received: August 10, 2023
Accepted manuscript online: September 8, 2023
Version of record online: September 14, 2023